Elastic wave mode separation for TTI media

Jia Yan and Paul Sava
Center for Wave Phenomena, Colorado School of Mines

ABSTRACT
The separation of wave modes for isotropic elastic wavefields is typically done using Helmholtz decomposition. However, Helmholtz decomposition using conventional divergence and curl operators does not give satisfactory results in anisotropic media and leaves the different wave modes only partially separated. The separation of anisotropic wavefields requires the use of more sophisticated operators which depend on local material parameters. Wavefield separation operators for TI (transverse isotropic) models can be constructed based on the polarization vectors evaluated at each point of the medium by solving the Christoffel equation using local medium parameters. These polarization vectors can be represented in the space domain as localized filters, which resemble conventional derivative operators. The spatially-variable "pseudo" derivative operators perform well in 2D heterogeneous TI media even at places of rapid variation. Wave separation for 3D TI media can be performed in a similar way. In 3D TI media, P and SV waves are polarized only in symmetry planes, and SH waves are polarized orthogonal to symmetry planes. Using the mutual orthogonality property between these modes, we only need to solve for the P wave polarization vectors from the Christoffel equation, and SV and SH wave polarizations can be constructed using the relationship between these three modes. Synthetic results indicate that the operators can be used to separate wavefields for TI media with arbitrary strength of anisotropy.

Key words: elastic, imaging, TTI, heterogeneous

1 INTRODUCTION

wave-equation migration for elastic data usually consists of two steps. The first step is wavefield reconstruction in the subsurface from data recorded at the surface. The second step is the application of an imaging condition which extracts reflectivity information from the reconstructed wavefields.

The elastic wave-equation migration for multicomponent data can be implemented in two ways. The first approach is to separate recorded elastic data into the compressional and transverse (P and S) modes and use these separated modes for acoustic wave-equation migration respectively. This acoustic imaging approach to elastic waves is used most frequently, but it is fundamentally based on the assumption that P and S data can be successfully separated on the surface, which is not always true (Etgen, 1988; Zhe & Greenhalgh, 1997). The second approach is to not separate P and S modes on the surface, extrapolate the entire elastic wavefield at once, then separate wave modes prior to applying an imaging condition. The reconstruction of elastic wavefields can be implemented using various techniques, including reconstruction by time reversal (RTM) (Chang & McMechan, 1986, 1994) or by Kirchhoff integral techniques (Hokstad, 2000).

The imaging condition applied to the reconstructed vector wavefields directly determines the quality of the images. The conventional cross-correlation imaging condition does not separate the wave modes and cross-correlates the Cartesian components of the elastic wavefields. In general, the various wave modes (P and S) are mixed on all wavefield components and cause crosstalk and image artifacts. Yan & Sava (2008b) suggest using imaging conditions based on elastic potentials, which require cross-correlation of separated modes. Potential-based imaging condition creates images that have a clear physical meaning, in contrast to images obtained with Cartesian wavefield components, thus justifying the need for wave mode separation.

As the need for anisotropic imaging increases, processing and migration are performed more frequently based on anisotropic acoustic one-way wave equations (Alkhalifah, 1998, 2000; Shan, 2006; Shan & Biondi, 2005; Fletcher et al., 2008). However, less research has been done on anisotropic elastic migration based on two-way wave equations. Elastic Kirch-

hoff migration (Hokstad, 2000) obtains pure-mode and converted mode images by downward continuation of elastic vector wavefields with a viscoelastic wave equation. The wavefield separation is effectively done with elastic Kirchhoff integration, which handles both P and S waves. However, Kirchhoff migration does not perform well in areas of complex geology where ray theory breaks down (Gray et al., 2001), thus requiring migration with more accurate methods, such as reverse time migration.

One of the complexities that impedes anisotropic migration using elastic wave equations is the difficulty in separating anisotropic wavefields into different wave modes after we reconstruct the elastic wavefields. However, the proper separation of anisotropic wave modes is as important for anisotropic elastic migration as the separation of isotropic wave modes is for isotropic elastic migration. Wave mode separation for isotropic media can be achieved by applying Helmholtz decomposition to the vector wavefields (Aki & Richards, 2002), which works for both homogeneous and heterogeneous isotropic media. Dellinger & Etgen (1990) extend the wave mode separation to homogeneous VTI (vertically transversely isotropic) media, where P and SV modes are obtained by projecting the vector wavefields onto the correct polarization vectors. Yan & Sava (2008a) apply this technology to heterogeneous VTI media and show that the method works if locally varying filters are used. even for complex geology with high heterogeneity,

However, VTI models are only suitable for limited geological settings with horizontal layering. TTI (tilted transversely isotropic) models characterize more general geological settings like thrusts and fold belts. Many case studies have shown that TTI models are good representations of complex geology, e.g., in the Canadian Foothills (Godfrey, 1991). Using the VTI assumption to imaging structures characterized by TTI anisotropy introduces image errors both kinematically and dynamically (Zhang & Zhang, 2008; Behera & Tsvankin, 2009). For example, Vestrum et al. (1999), Isaac & Lawyer (1999), and Behera & Tsvankin (2009) show that seismic structures can be mispositioned if isotropy, or even VTI anisotropy, is assumed when the medium above the imaging targets is TTI. Therefore, in order for the separation to work for more general TTI models, the wave mode separation algorithm needs to be adapted to TTI media. For sedimentary layers bent under geological forces, the modeling/migration model also needs to incorporate locally varying tilts that are consistent with the local beddings, under the assumption that the local symmetry axis of the model is orthogonal to the reflectors throughout the model. Because the symmetry axis varies from place to place, it is essential to use spatially-varying filters to separate the wave modes in complex TI models.

To date, separation of elastic wave modes based on computing polarization vectors has been applied only to 2D VTI models (Dellinger, 1991; Yan & Sava, 2008a) and P wave mode separation for 3D anisotropic models (Dellinger, 1991). Conventionally, 3D elastic wavefields are usually first separated into in-plane (P and SV waves) and out-of-plane components (SH wave); then the in-plane wavefields can be separated into P and SV modes using conventional Helmholtz decomposition for isotropic media or pseudo-derivative operators for symmetry planes in VTI media (Yan & Sava, 2008a). However, this procedure requires slicing the elastic wavefields along the planes of symmetry. This involves interpolation of the wavefields because 3D wavefields are modeled in Cartesian coordinates, while the slicing of wavefields into symmetry planes implies cylindrical coordinates. Furthermore, it is difficult to determine the optimum number of azimuths for this procedure. In contrast to this procedure, we propose a new technique to separate 3D elastic wavefields for TI media with 3D separators all, which reduces the need for interpolation of 3D wavefields.

This paper first reviews the wave mode separation for 2D VTI media and then extends the algorithm to symmetry planes of TTI media. Then, we generalize this approach to the wave mode separation in 3D TI media. We illustrate the separation for 2D TTI media with two realistic synthetic examples. Finally, we demonstrate 3D elastic wave mode separation in homogeneous isotropic and VTI models.

2 WAVE MODE SEPARATION FOR 2D TI MEDIA

Dellinger & Etgen (1990) suggest that wave mode separation of *quasi*-P and *quasi*-SV modes in 2D VTI media can be done by projecting the wavefields onto the directions in which the P and S modes are polarized. For example, we can project the wavefields onto the P wave polarization directions $\mathbf{U}_P$ to obtain *quasi*-P (*q*P) waves:

$$\widetilde{qP} = i\,\mathbf{U}_P(\mathbf{k}) \cdot \widetilde{\mathbf{W}} = i\,U_x\,\widetilde{W}_x + i\,U_z\,\widetilde{W}_z\,, \qquad (1)$$

where $\widetilde{qP}$ is the P wave mode in the wavenumber domain, $\mathbf{k} = \{k_x, k_z\}$ is the wavenumber vector, $\widetilde{\mathbf{W}}$ is the elastic wavefield in the wavenumber domain, and $\mathbf{U}_P(k_x, k_z)$ is the P wave polarization vector as a function of $\mathbf{k}$. Generally, in anisotropic media, $\mathbf{U}_P(k_x, k_z)$ deviates from $\mathbf{k}$, as illustrated in Figure 1, which shows the polarization vectors of *q*P wave mode for a VTI and a TTI model, respectively. Figure 2(a) shows the P wave polarization vectors projected on the z and x directions, as a function of normalized k_x and k_z ranging from $-\pi$ to π radians.

Dellinger & Etgen (1990) demonstrate wave mode separation in the wave number domain using projection of the polarization vectors, as indicated by equation 1. However, for heterogeneous media, this procedure does not perform well because the polarization vectors are spatially varying. We can write an equivalent expression to equation 1 in the space domain at each grid point (Yan & Sava, 2008a):

$$qP = \nabla_a \cdot \mathbf{W} = L_x[W_x] + L_z[W_z]\,, \qquad (2)$$

where L_x and L_z represent the inverse Fourier transforms of $i\,U_x$ and $i\,U_z$, and $L\,[\,]$ represents spatial filtering of the wavefield with anisotropic separators. L_x and L_z define pseudo-derivative operators in the x and z directions for a 2D VTI

medium in the symmetry plane, and they can change from location to location according to the material parameters.

The separation of P and SV wavefields can be similarly accomplished for both VTI and TTI media. However, the filters for TTI and VTI media are different. The main difference is that for VTI media, waves propagating in all vertical planes are simply P and SV wave modes. However, for TTI media, only P and SV wave modes are polarized in the vertical symmetry plane, and SH waves are decoupled from P and SV modes, while in other vertical planes, the propagating waves are a mix of P, SV, and SH modes. Therefore, the 2D wave mode separation works for the vertical symmetry plane or other non-vertical symmetry planes of TTI media.

For a medium with arbitrary anisotropy, we obtain the polarization vectors $\mathbf{U}(\mathbf{k})$ by solving the Christoffel equation (Aki & Richards, 2002; Tsvankin, 2005):

$$\left[\mathbf{G} - \rho V^2 \mathbf{I}\right] \mathbf{U} = 0\,, \tag{3}$$

where $\mathbf{G}$ is the Christoffel matrix with $G_{ij} = c_{ijkl} n_j n_l$, in which c_{ijkl} is the stiffness tensor, n_j and n_l are the normalized wave vector components in the j and l directions with $i, j, k, l = 1, 2, 3$. The parameter V corresponds to the eigenvalues of the matrix $\mathbf{G}$ and represents the phase velocities of different wave modes as functions of the wave vector $\mathbf{k}$ (corresponding to n_j and n_l in the matrix $\mathbf{G}$). For plane waves propagating in a symmetry plane of a TTI medium, since qP and qSV modes are decoupled from the SH mode and polarized in the symmetry planes, we can set $k_y = 0$ and get

$$\begin{bmatrix} G_{11} - \rho V^2 & G_{12} \\ G_{12} & G_{22} - \rho V^2 \end{bmatrix} \begin{bmatrix} U_x \\ U_z \end{bmatrix} = 0\,, \tag{4}$$

where

$$G_{11} = c_{11} k_x^2 + 2 c_{15} k_x k_z + c_{55} k_z^2\,, \tag{5}$$

$$G_{12} = c_{15} k_x^2 + (c_{13} + c_{55})\, k_x k_z + c_{35} k_x^2\,, \tag{6}$$

$$G_{22} = c_{55} k_x^2 + 2 c_{35} k_x k_z + c_{33} k_z^2\,. \tag{7}$$

This equation allows us to compute the polarization vectors $\mathbf{U}_P = \{U_x, U_z\}$ and $\mathbf{U}_{SV} = \{-U_z, U_x\}$ (the eigenvectors of the matrix) for P and SV wave modes given the stiffness tensor at every location of the medium. Here, the symmetry axis of the TTI medium is not aligned with vertical axis of the Cartesian coordinates, and the TTI Christoffel matrix takes a different form than the VTI form.

Figure 2(b) shows the z and x components of the P wave polarization vectors of a TTI medium with a 30° tilt angle, and Figure 2(c) shows the polarization vectors projected onto the symmetry axis and the isotropy plane (30° and -60°). Comparing Figure 2(a) and 2(c), we see that the polarization vectors of this TTI medium are rotated 30° from those of the VTI medium. However, notice that: the z and x components of the polarization vectors for the VTI medium, Figure 2(a), are symmetric with respect to x and z axes, respectively; while the polarization vector components for the TTI medium, Figure 2(c), are not.

In order to maintain the continuity at the negative and positive Nyquist wavenumbers, $-\pi$ and π radians, we apply a taper to the vector components. For VTI media, a taper corresponding to the function (Yan & Sava, 2008a)

$$f(k) = -\frac{8\sin(k)}{5k} + \frac{2\sin(2k)}{5k} - \frac{8\sin(3k)}{105k} + \frac{\sin(4k)}{140k} \tag{8}$$

can be applied to the x and z components of the polarization vectors. The taper ensures that the Fourier domain derivatives are 0 at the positive and negative Nyquist wavenumbers in the derivative directions. They are also continuous in the z and x directions, respectively, due to the symmetry. The taper applied to isotropic polarization vectors $\mathbf{k}$ leads to the normal finite difference operators in the space domain (Yan & Sava, 2008a). Therefore, the VTI operators degenerate to normal derivatives $\frac{\partial}{\partial x}$ and $\frac{\partial}{\partial z}$ when the anisotropic parameters ϵ and δ are both zero.

For TTI media, due to the asymmetry of the Fourier domain derivatives, we need to apply a rotational symmetric taper to the polarization vector components. A simple Gaussian taper

$$f(k) = Exp\left[-\frac{||\mathbf{k}||^2}{2\sigma^2}\right] \tag{9}$$

can be applied to both components of TTI media polarization vectors. We choose a standard deviation of $\sigma = 1$. In this case, at the positive and negative Nyquist wavenumbers ($-\pi$ and π radians), the magnitude of this taper is about 3% of the peak value, and the components can be safely assumed to be continuous across the Nyquist wavenumbers. However, after applying this taper, even for isotropic media, the space domain derivatives are not the conventional finite difference operators. Compared to conventional finite difference operators which are 1D stencils, the derivatives constructed after the application of the Gaussian taper are represented by 2D stencils.

Figure 3 illustrates the application of the Gaussian taper to the polarization vectors shown in Figure 2. Figures 3(a), 4(a) and Figures 3(b), 4(b) are the k and x domain representations of the polarization vector components for the VTI medium and the TTI medium after applying the Gaussian taper, respectively; Figures 3(c) and 4(c) are the polarization vectors projected on the symmetry axis and isotropy plane of the TTI medium. We see that the derivatives in the k domain are now continuous across the Nyquist wavenumbers in both x and z directions, and that the x domain derivatives are 2D compared to the conventional 1D finite difference operators.

We can apply the procedure described here to heterogeneous media by computing two different operators, namely U_x and U_z, at every grid point. In any symmetry plane of a TTI medium, the operators are 2D and depend on the local values of the stiffness coefficients. For each point, we pre-compute the polarization vectors as a function of the local medium parameters and transform them to the space domain to obtain the wave mode separators. We assume that the medium parameters vary smoothly (locally homogeneous), but even for complex media, the localized operators work similarly as the long finite difference operators would work for locations where medium parameters change rapidly.

If we represent the stiffness coefficients using Thomsen

parameters (Thomsen, 1986), then the pseudo-derivative operators L_x and L_z depend on ϵ, δ, V_P/V_S ratio along the symmetry axis and title angle ν, all of which can be spatially varying. We can compute and store the operators for each grid point in the medium and then use these operators to separate P and S modes from reconstructed elastic wavefields at different time steps. Thus, wavefield separation in TI media can be achieved simply by non-stationary filtering with operators L_x and L_z.

3 WAVE MODE SEPARATION FOR 3D TI MEDIA

Since SV and SH waves have the same velocity along the symmetry axis in 3D TI media, it is not possible to obtain the shear mode polarization vectors in this particular direction by solving the Christoffel equation. This point is known by the name "kiss singularity" (Tsvankin, 2005). For a point source in 3D TI media, S wave modes near the singularity directions have complicated nonlinear polarization that cannot be characterized by a plane wave solution. Consequently, the polarization vectors for both fast and slow S modes have singularities in the symmetry direction, and we cannot construct 3D global separators for both S waves based on the 3D Christoffel solution to the TI elastic wave equation. However, the P wave mode is always well-behaved and does not have the problem of singularity. Therefore, for 3D TI media, we can always construct a P wave separator represented by the polarization vector $\mathbf{U}_P = \{U_x, U_y, U_z\}$. We obtain the P mode by projecting the 3D elastic wavefields onto the vector $\mathbf{U}_P$.

Here, we consider a 3D VTI medium. The P wave polarization $\{U_x, U_y, U_z\}$ is obtained by solving the 3D Christoffel matrix (Tsvankin, 2005):

$$\begin{bmatrix} G_{11}-\rho V^2 & G_{12} & G_{13} \\ G_{12} & G_{22}-\rho V^2 & G_{23} \\ G_{13} & G_{23} & G_{33}-\rho V^2 \end{bmatrix} \begin{bmatrix} U_x \\ U_y \\ U_z \end{bmatrix} = 0\,, \tag{10}$$

where

$$\begin{aligned} G_{11} &= c_{11}k_x^2 + c_{66}k_x^2 + c_{55}k_x^2\,, && (11)\\ G_{22} &= c_{66}k_x^2 + c_{22}k_x^2 + c_{44}k_x^2\,, && (12)\\ G_{33} &= c_{55}k_x^2 + c_{44}k_x^2 + c_{33}k_x^2\,, && (13)\\ G_{12} &= (c_{11}+c_{66})k_xk_y\,, && (14)\\ G_{13} &= (c_{13}+c_{55})k_xk_z\,, && (15)\\ G_{23} &= (c_{23}+c_{44})k_yk_z\,. && (16) \end{aligned}$$

We artificially remove the S wave mode singularity by using the relative P-SV-SH mode polarization orthogonality in the cylindrical system. In every vertical plane of the 3D VTI model, SV and SH mode polarization are defined to be perpendicular to the P mode in and out of the propagation plane. Figure 5(a) depicts a schematic showing how P, SV, and SH modes are polarized at an arbitrary oblique propagation angle. For this 3D VTI medium, without losing generality, the symmetry axis ($\mathbf{n}$) can be expressed by $\mathbf{n} = \{0,0,1\}$; and the propagation plane of all the elastic plane waves is the plane that contains the symmetry axis and the line connecting the source ($\mathbf{S}$) and an arbitrary point in space ($\mathbf{x}$). Due to the rotational symmetry of VTI media, P and SV waves are only polarized in this propagation plane, and the SH wave is polarized perpendicular to this plane. We can first calculate the SH wave polarization $\mathbf{U}_{SH}$ by

$$\begin{aligned} \mathbf{U}_{SH} &= \mathbf{n}\times\mathbf{U}_P \\ &= \{0,0,1\}\times\{U_x,U_y,U_z\} \\ &= \{-U_y,U_x,0\}. \end{aligned} \tag{17}$$

Then we can calculate the SV polarization $\mathbf{U}_{Sv}$ by

$$\begin{aligned} \mathbf{U}_{SV} &= \mathbf{U}_P\times\mathbf{U}_{SH}\,, \\ &= \{U_x,U_y,U_z\}\times\{-U_y,U_x,0\}\,, \\ &= \{-U_xU_z,-U_yU_z,U_x^2+U_y^2\}\,. \end{aligned} \tag{18}$$

Here, the P wave polarization vectors are normalized

$$U_x^2 + U_y^2 + U_z^2 = 1\,. \tag{19}$$

The polarization for P, SV, and SH mode are shown in Figure 6.

Suppose that the vector wavefields $\mathbf{W} = \{W_x, W_y, W_z\}$ in the k domain include all three elastic wave modes P, SV, and SH. Then each component of the vector wavefields is composed of all these elastic modes projected onto their respective normalized polarization directions. We can express the vector wavefields $\mathbf{W}$ as:

$$\widetilde{W}_x = PU_x + SV\frac{-U_xU_z}{\sqrt{U_x^2+U_y^2}} + SH\frac{-U_y}{\sqrt{U_x^2+U_y^2}} \tag{20}$$

$$\widetilde{W}_y = PU_y + SV\frac{-U_yU_z}{\sqrt{U_x^2+U_y^2}} + SH\frac{U_x}{\sqrt{U_x^2+U_y^2}} \tag{21}$$

$$\widetilde{W}_z = PU_z + SV\,. \tag{22}$$

Here, P, SV, and SH are the magnitude P, SV, and SH mode in the k domain, respectively. Note that all the wave modes are projected onto their normalized polarization vectors. We can confirm that, in the symmetry axis where $U_x = 0$ and $U_y = 0$, the SV and SH wave polarizations are not well-defined, which corresponds to the singularity mentioned earlier.

However, because we use un-normalized polarization vectors in Equations 17 and 18 to filter the wavefields, the polarization vectors in the vertical propagation direction become

$$\begin{aligned} \mathbf{U}_P &= \{0,0,U_z\}\,, \\ \mathbf{U}_{SV} &= \{0,0,0\}\,, \\ \mathbf{U}_{SH} &= \{0,0,0\}\,. \end{aligned} \tag{23}$$

The magnitude of both SV and SH waves becomes zero in the singularity direction. This procedure naturally avoids the singularity problem which impedes us from constructing 3D separators for S modes. The zero amplitude of S wave modes in the vertical direction is not abrupt but a continuous change over nearby propagation angles.

We can verify that the P wave is obtained by

$$\begin{aligned} \widetilde{qP} &= i\,\mathbf{U}_P(\mathbf{k})\cdot\widetilde{\mathbf{W}} \\ &= i\,U_x\,\widetilde{W}_x + i\,U_y\,\widetilde{W}_y + i\,U_z\,\widetilde{W}_z \\ &= P\,, \end{aligned} \tag{24}$$

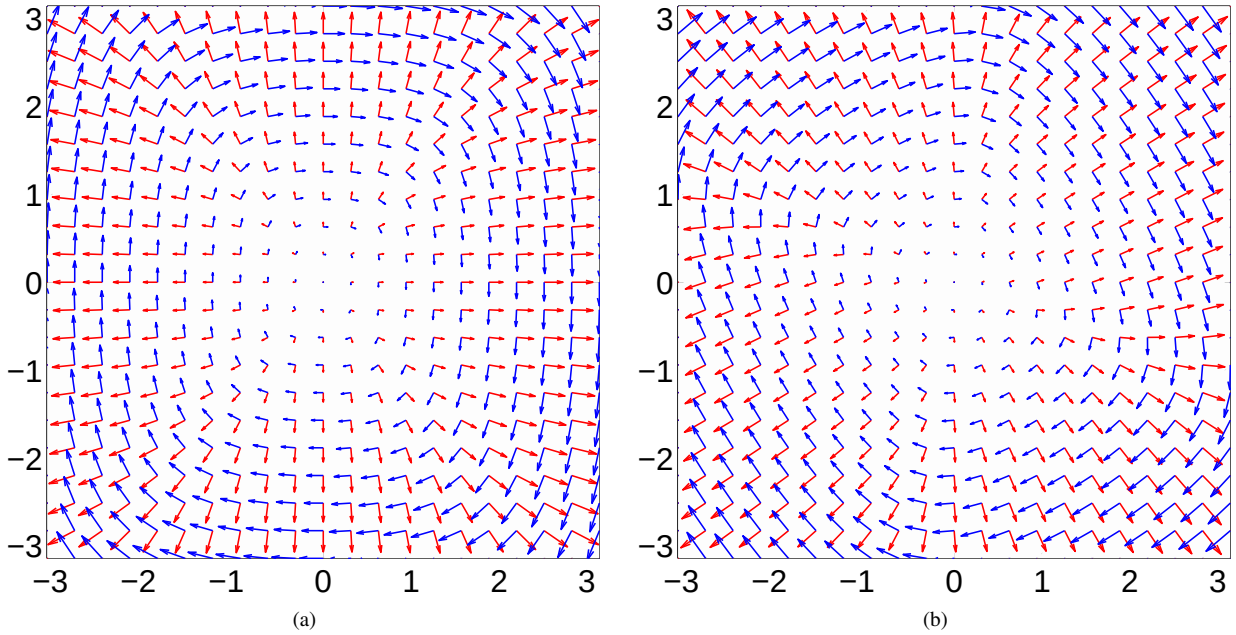


Figure 1. The qP and qS polarization vectors as a function of normalized wavenumbers k_x and k_z ranging from -1 to $+1$ cycles, for (a) a VTI model with $V_{P0} = 3$ km/s, $V_{S0} = 1.5$ km/s, $\epsilon = 0.25$ and $\delta = -0.29$ (b) a TTI model with the same model parameters as (a) and a symmetry axis tilt $\nu = 30^\circ$. The arrows in almost radial directions are the qP wave polarization vectors, and the arrows in almost tangential directions are the qS wave polarization vectors.

the SV wave is obtained by

$$\begin{aligned} \widetilde{qSV} &= i\,\mathbf{U}_{SV}(\mathbf{k}) \cdot \widetilde{\mathbf{W}} \\ &= -i\,U_x U_z\,\widetilde{W}_x - i\,U_y U_z\,\widetilde{W}_y + i\,(U_x^2 + U_y^2)\,\widetilde{W}_z \\ &= SV\sqrt{U_x^2 + U_y^2}\,, \end{aligned} \tag{25}$$

and the SH wave is obtained by

$$\begin{aligned} \widetilde{qSH} &= i\,\mathbf{U}_{SH}(\mathbf{k}) \cdot \widetilde{\mathbf{W}} \\ &= -i\,U_y\,\widetilde{W}_x + i\,U_x\,\widetilde{W}_y \\ &= SH\sqrt{U_x^2 + U_y^2}\,. \end{aligned} \tag{26}$$

We can see that SV and SH waves are scaled differently than the P wave. The SV and SH waves are scaled by the magnitude $\sqrt{U_x^2 + U_y^2}$, which more or less characterizes wave propagation directions. This scaling factor goes from zero in the vertical propagation direction to unity in the horizontal propagation directions.

For general 3D TI media whose symmetry axis has non-zero tilt and azimuth, we simply need to represent the symmetry-axis vector as $\{\sin\nu\cos\alpha, \sin\nu, \sin\alpha, \cos\nu\}$, where ν and α are the symmetry axis tilt and azimuth angles, respectively (Figure 5(b)). The P wave polarization can be computed from the TTI Christoffel equation, and SH and SV wave polarizations can be calculated from P wave polarization and the symmetry axis vector using the orthogonality between these modes.

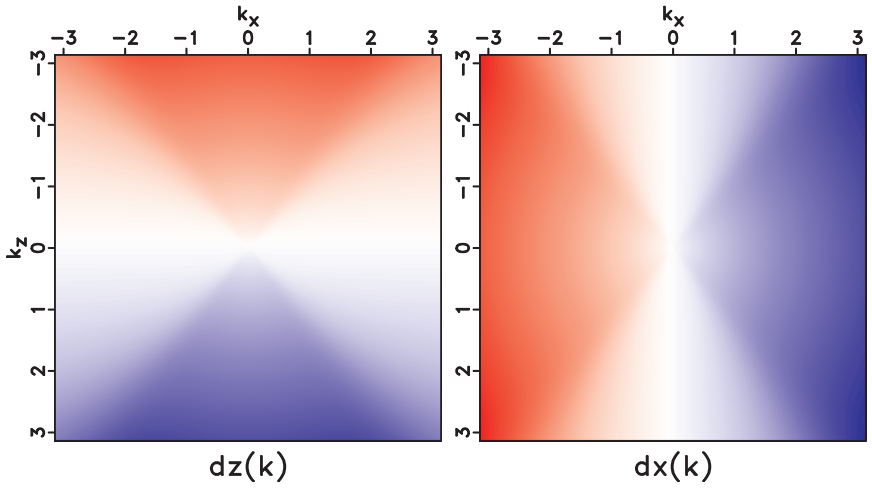
The wave polarization vectors for P, SV, and SH waves can be brought to space domain to construct spatial filters for 3D heterogeneous TI media. Therefore, wave mode separation would work for models that have complex structures and tributary tilts of TI symmetry.

4 EXAMPLES

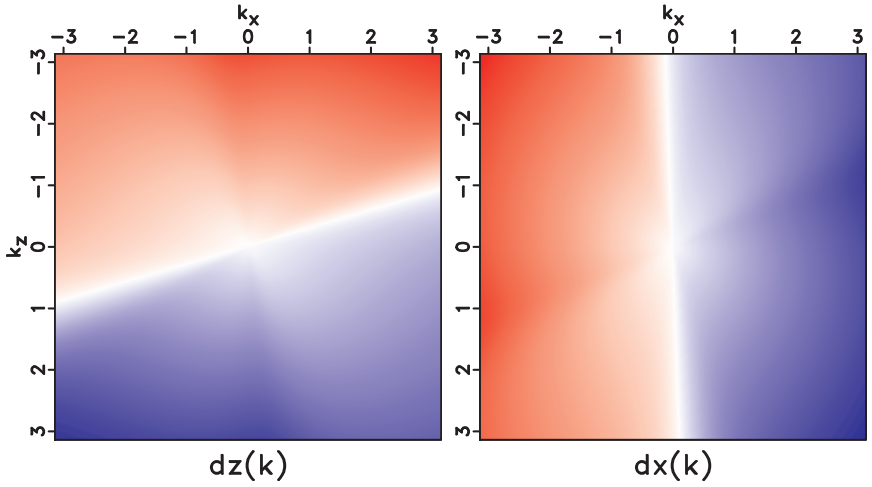
We illustrate the anisotropic wave mode separation with a simple fold synthetic example and a more challenging elastic model based on the elastic Marmousi II model (Bourgeois et al., 1991). We then show the wave mode separation for a 3D isotropic model and a 3D VTI model.

4. 1 2D TTI fold model

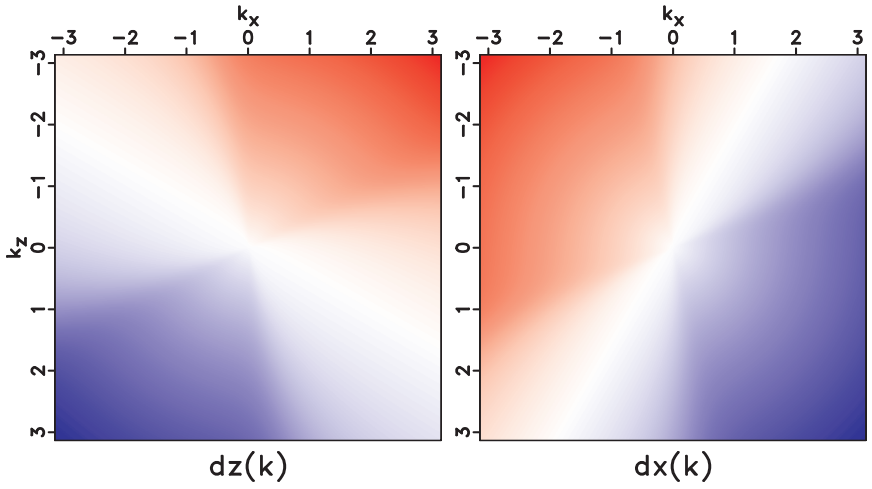
We consider the 2D TTI model shown in Figure 7. Panels 7(a) to 7(f) shows the P and S wave velocities along the local symmetry axis, parameters ϵ, δ and the local tilts ν of the model, respectively. The symmetry axis is orthogonal to the reflectors throughout the model. Figure 8 illustrates the pseudo-derivative operators obtained at different locations in the model defined by the intersections of x coordinates $0.15, 0.3, 0.45$ km and z coordinates $0.15, 0.3, 0.45$ km, shown by the dots in Figure 7(f). The operators are projected onto their local symmetry axis and the isotropy plane (the direction orthogonal to it). Since the operators correspond to different combinations of V_P/V_S ratio along the symmetry axis and parameters ϵ, δ and tilt angle ν, they have different forms.



(a)

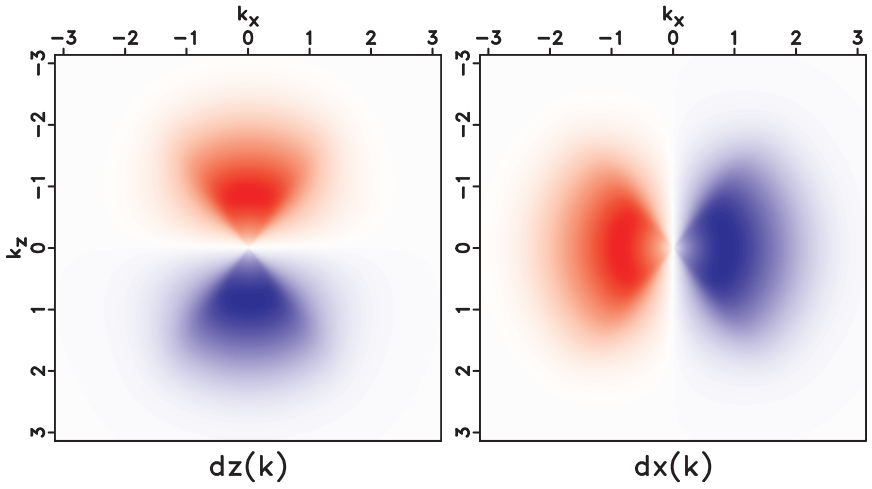


(b)

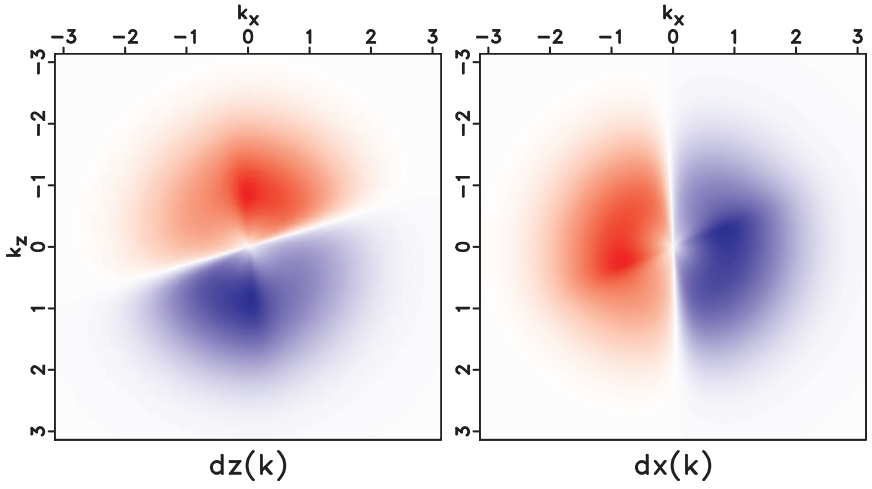


(c)

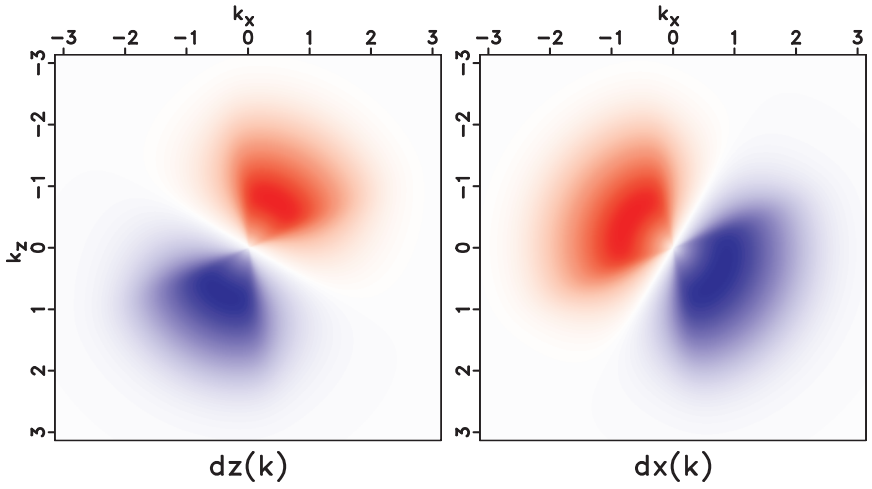
Figure 2. Polarization vectors in the Fourier domain for (a) a VTI medium with $\epsilon = 0.25$ and $\delta = -0.29$, (b) a TTI medium with $\epsilon = 0.25$, $\delta = -0.29$ and $\nu = 30^\circ$. Panel (c) represents the projection of the polarization vectors shown in (b) onto the tilt axis and the isotropy plane.



(a)

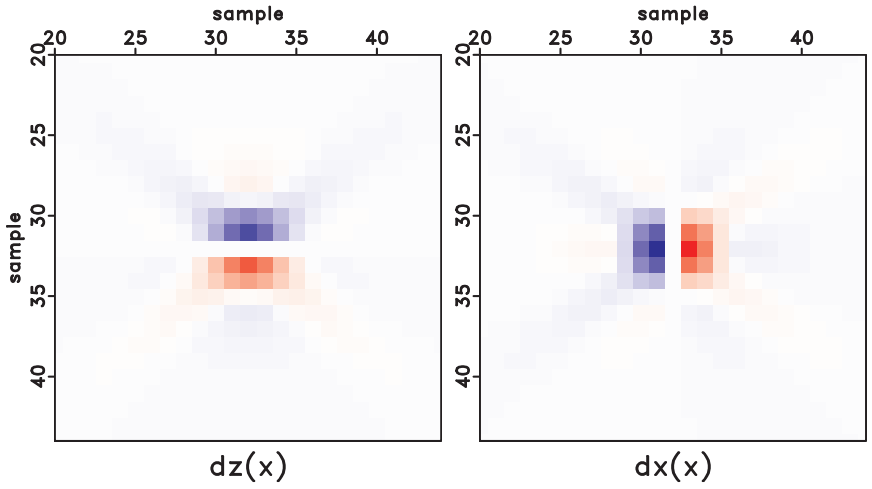


(b)

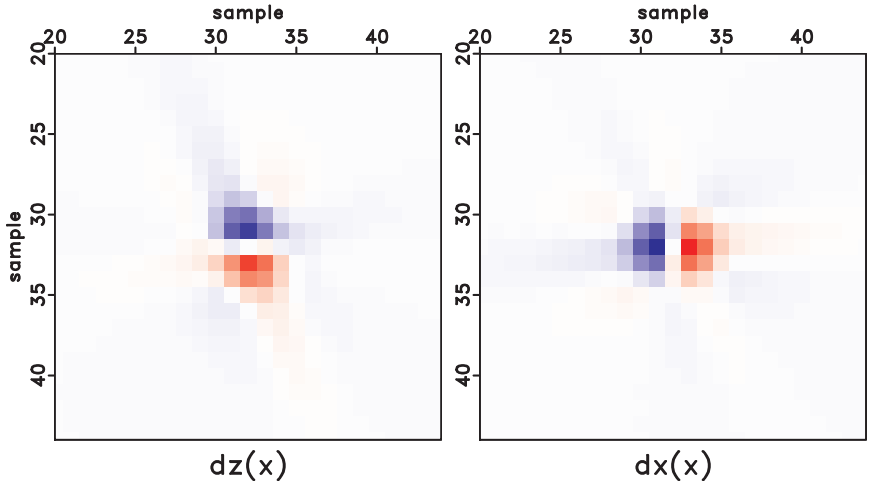


(c)

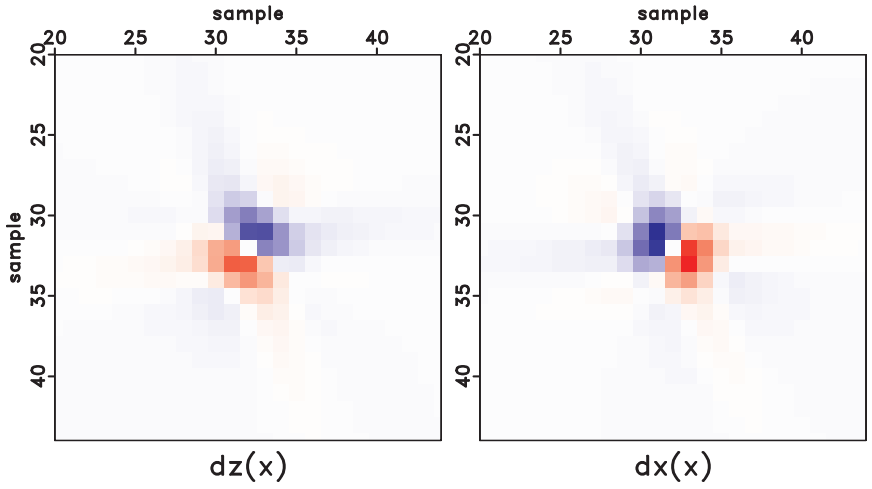
Figure 3. The polarization vectors in the wavenumber domain for the models shown in Figure 2. The wavenumber domain vectors are tapered by the function $Exp\left[-\frac{k_x^2+k_z^2}{2}\right]$ to avoid Nyquist discontinuity. Panel (a) corresponds to the VTI medium, panel (b) corresponds to the TTI medium, and panel (c) is the projection of the polarization vectors shown in (b) on the tilt axis and the isotropy plane.



(a)



(b)



(c)

Figure 4. The space domain wave mode separators for the media shown in Figure 2. They are the Fourier transformation of the polarization vectors shown in Figure 3. Panel (a) corresponds to the VTI medium, panel (b) corresponds to the TTI medium, and panel (c) is the projection of the polarization vectors shown in (b) on the tilt axis and the isotropy plane.

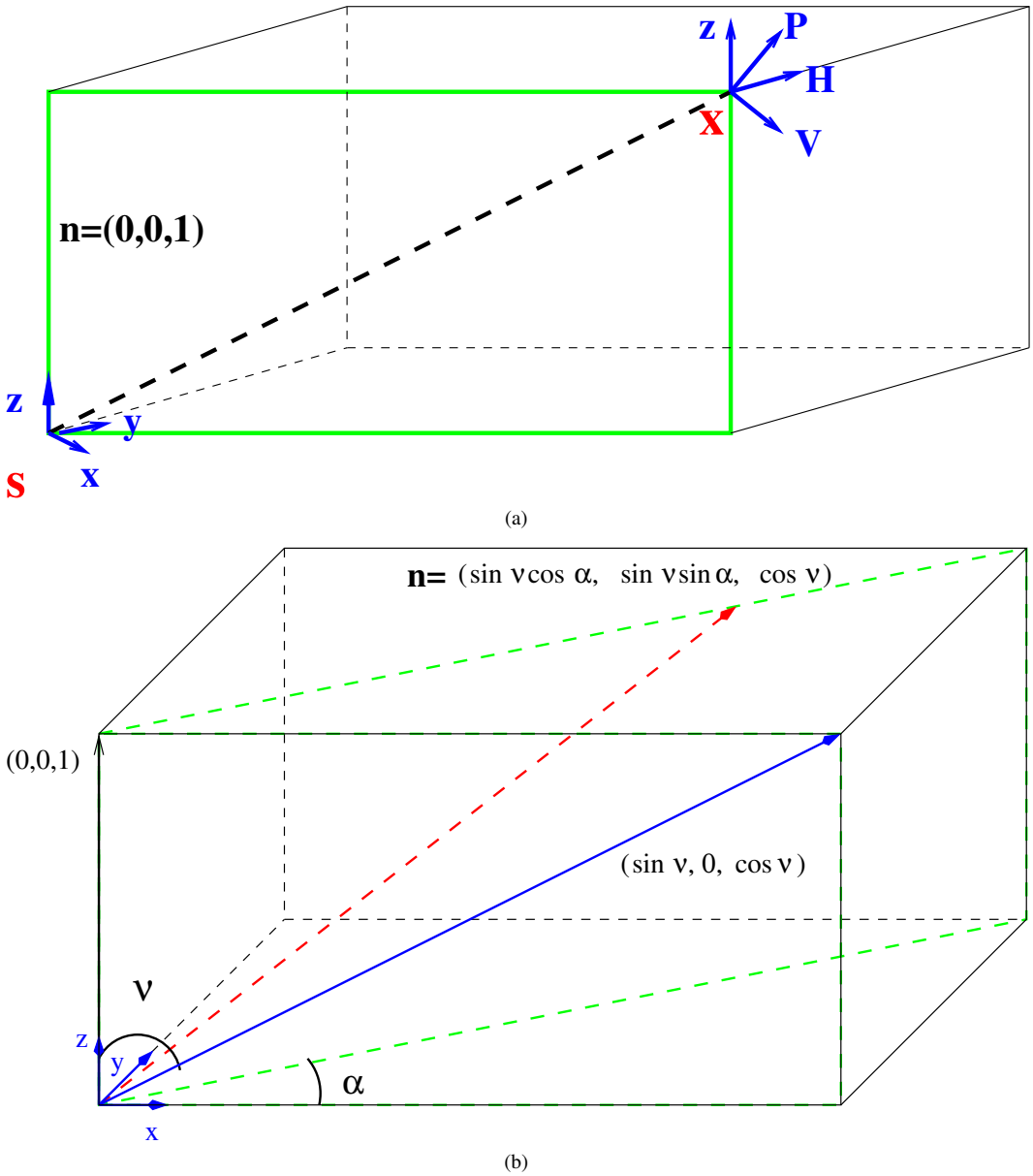


Figure 5. (a) A schematic showing the elastic wave modes polarization in a 3D VTI medium. **S** is the source, and **x** represents the coordinates of a spatial point. $\mathbf{n} = \{0, 0, 1\}$is the symmetry axis of the VTI medium. The wave mode P is polarized in the direction $\{U_x, U_y, U_z\}$, the wave mode SV is polarized in the direction $\{-U_x U_z, -U_y U_z, U_x^2 + U_y^2\}$, and the wave mode SH wave is polarized in the direction $\{-U_y, U_x, 0\}$. (b) A schematic showing the symmetry axis for a general TTI medium whose tilt and symmetry axis are both non-zero. The symmetry axis $=\{\sin\nu\cos\alpha, \sin\nu, \sin\alpha, \cos\nu\}$.

As we can see, the orientation of the operators conforms to the corresponding tilts at the locations shown by the dots in Figure 7(f).

Figure 9(a) shows the vertical and horizontal components of one snapshot of the simulated elastic anisotropic wavefield; Figure 9(b) shows the separation to qP and qS modes using VTI filters, i.e., by assuming zero tilt throughout the model; and Figure 9(c) shows the mode separation obtained with the correct TTI operators constructed using the local medium parameters with correct tilts. A comparison of Figure 9(b) and 9(c) indicates that the spatially-varying derivative operators with correct tilts successfully separate the elastic wavefields into qP and qS modes, while the VTI operators only work in the part of the model where it is locally VTI. The separation using VTI filters fails at locations where the local dip is large. For example, at coordinates $x = 0.42$ km and $z = 0.1$ km, we see strong S wave residual in the qP panel; and at coordinates

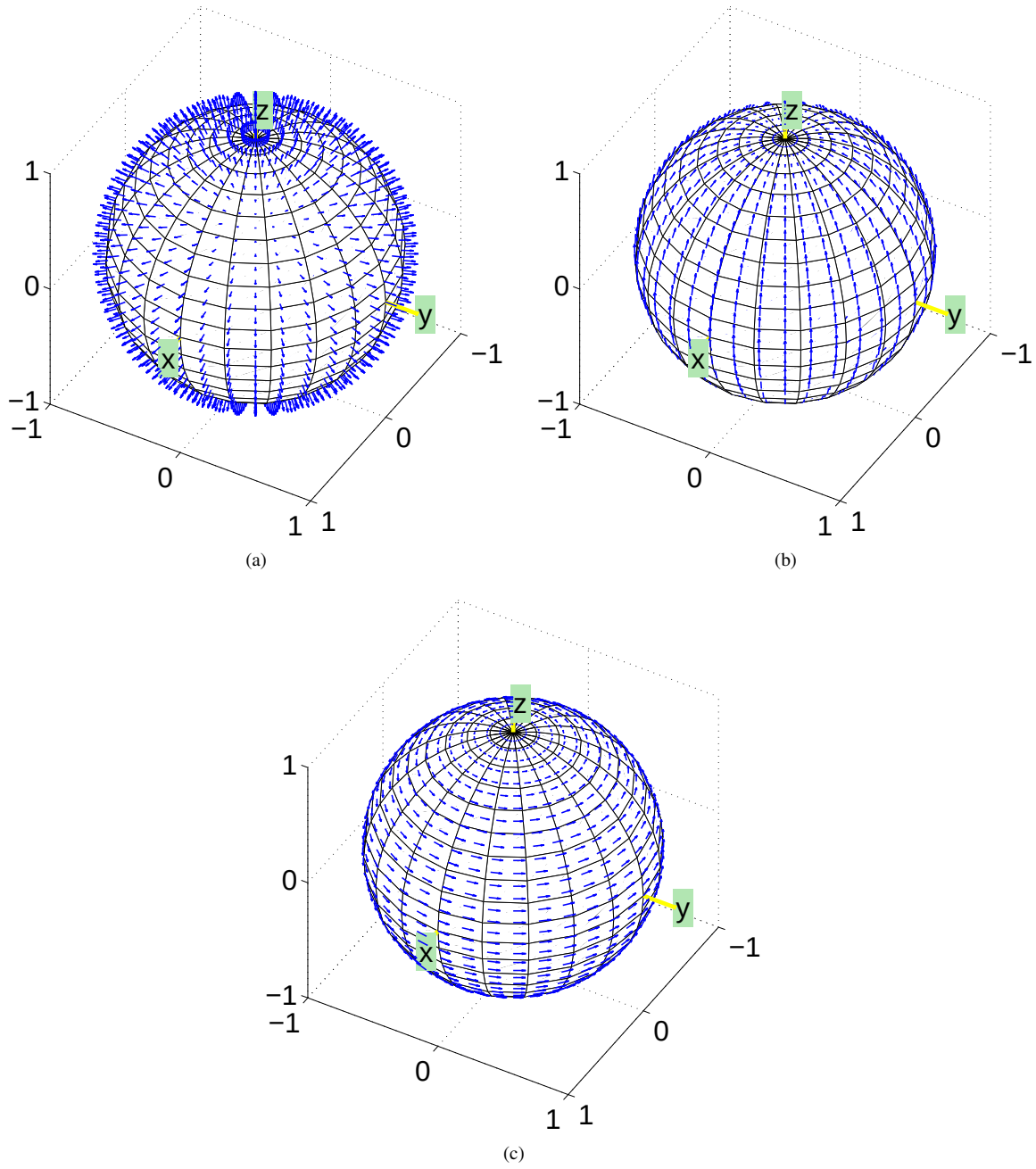


Figure 6. Panels (a) to (c) correspond to the wave mode polarization for P, SV, and SH mode for a VTI medium using Equations 18 and 17. Note that the SV and SH wave polarization vectors have zero amplitude in the vertical direction.

$x = 0.02$ km and $z = 0.1$ km, we see P wave residual in the qS panel.

4. 2 Marmousi II model

Our second model (Figure 10) uses an elastic anisotropic version of the Marmousi II model (Bourgeois et al., 1991). In our modified model, the P wave velocity (Figure 10(a)) is taken from the original model, the V_P/V_S ratio along the symmetry axis is two, the parameter ϵ ranges from 0.13 to 0.36 (Figure 10(d)), and parameter δ ranges from 0.11 to 0.24 (Figure 10(e)). Figure 10(f) represents the local dips of the model obtained from the density model using plane wave decomposition. The dip model is used to simulate the TTI wavefields and also used to construct wavefield separators. A displacement source oriented at 45° to the vertical direction is located

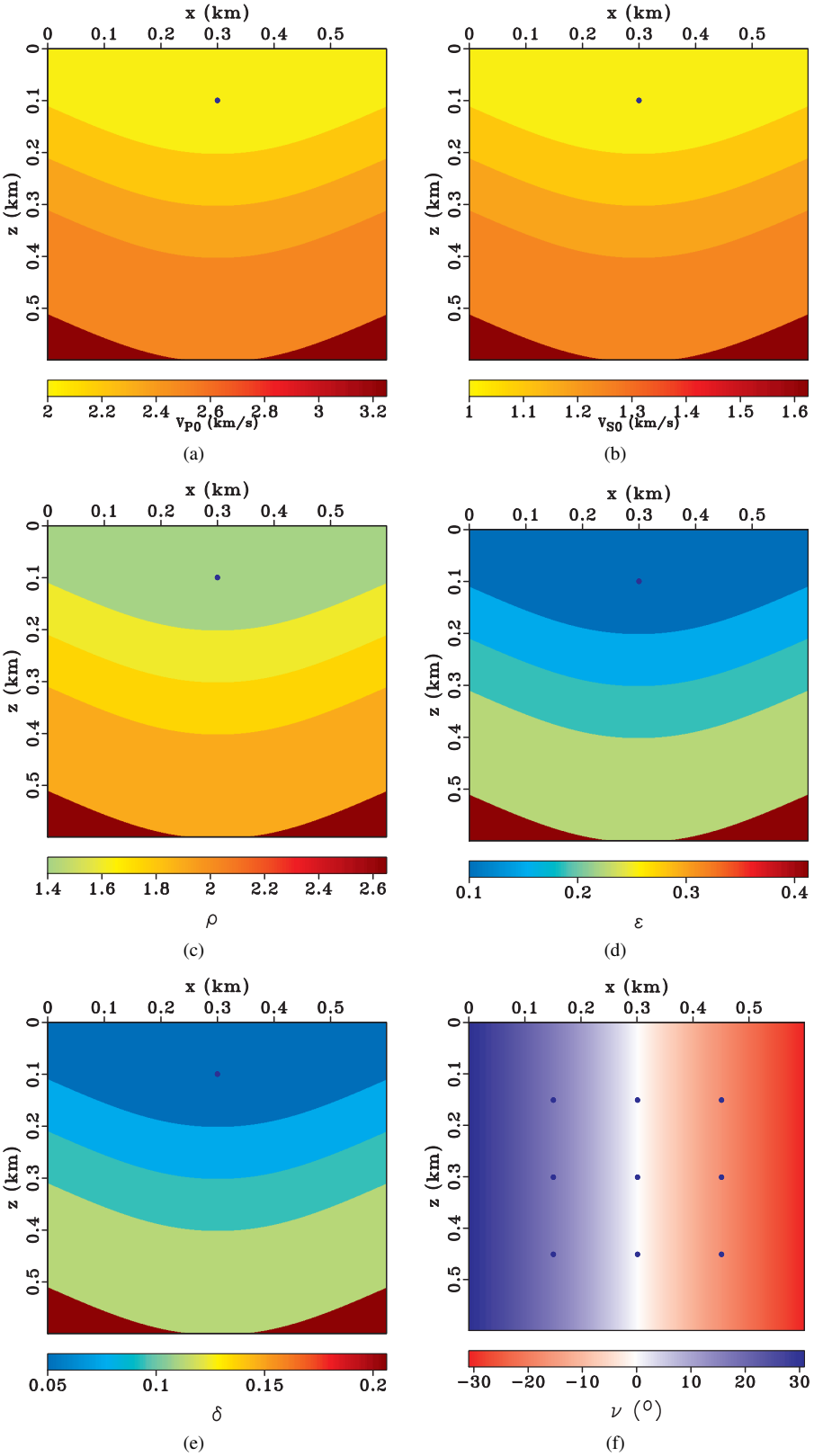


Figure 7. A fold model with parameters (a) P wave velocity along the local symmetry axis, (b) S wave velocity along the local symmetry axis, (c) density, (d) ϵ, (e) δ, and (f) tilt angle ν. A vertical point force source is located at $x = 0.3$ km and $z = 0.1$ km shown by the dot in panel (b) to (f). The dots in panel (f) correspond to the locations of the anisotropic operators shown in Figure 8.

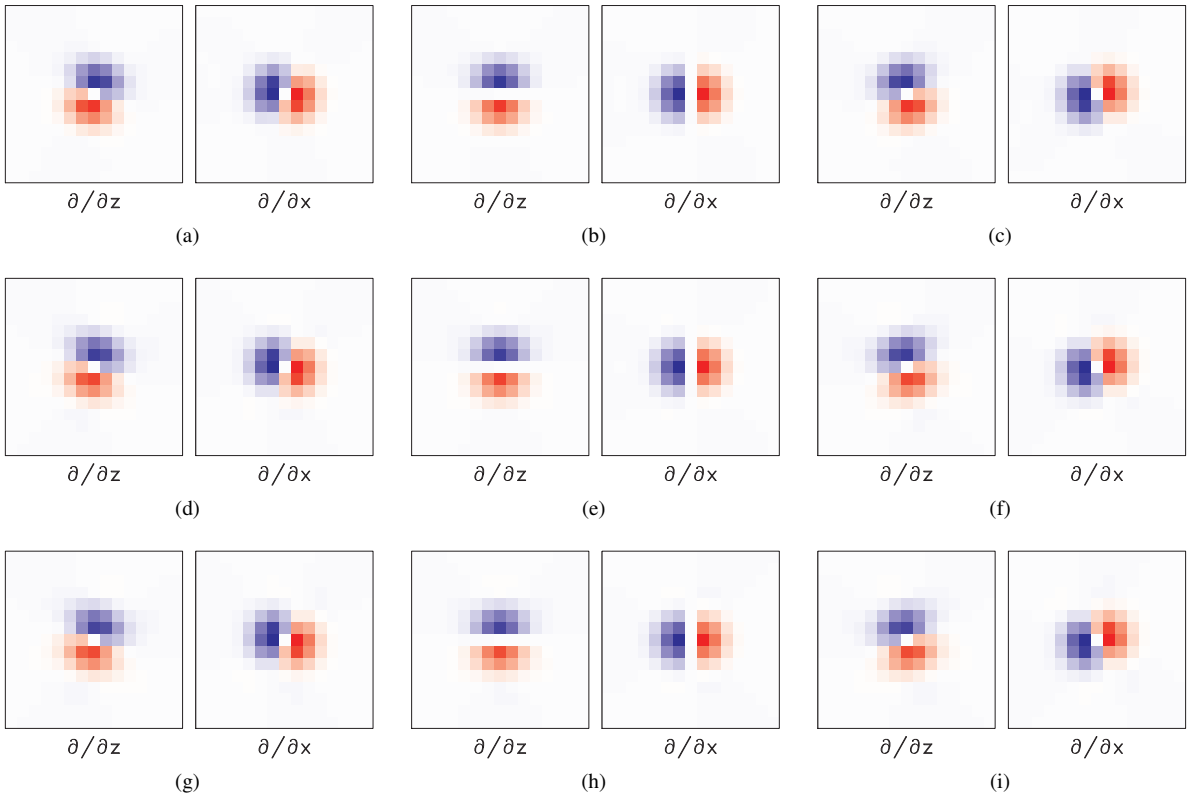


Figure 8. The TTI pseudo-derivative operators in the z and x directions at the intersections of $x = 0.15, 0.3, 0.45$ km and $z = 0.15, 0.3, 0.45$ km for the model shown in Figure 7.

at coordinates $x = 11$ km and $z = 1$ km to simulate the elastic anisotropic wavefield.

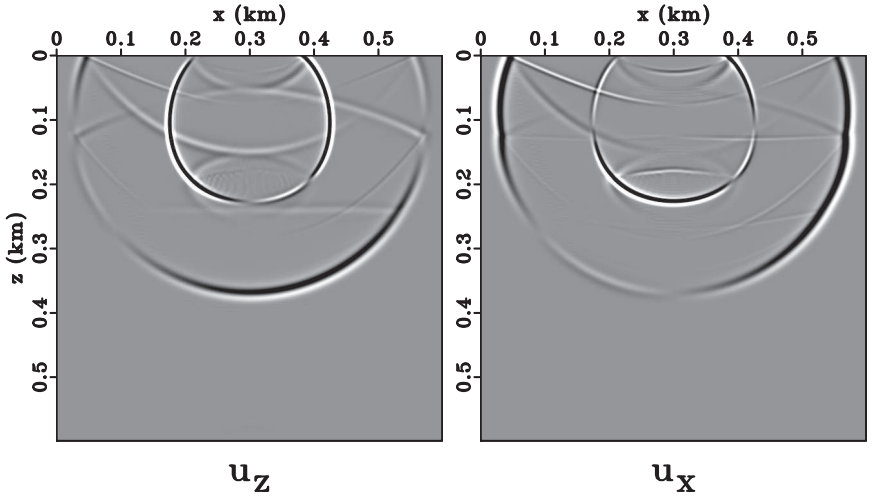
Figure 11(a) shows one snapshot of the simulated elastic anisotropic wavefields using the model shown in Figure 10. Figures 11(b), 11(c), and 11(d) show the separation using conventional $\nabla\cdot$ and $\nabla\times$ operators, VTI filters, and correct TTI filters, respectively. The VTI filters are constructed assuming zero tilt throughout the model, and the TTI filters are constructed using the dips used for modeling. As we expect, the conventional $\nabla\cdot$ and $\nabla\times$ operators fail at locations where anisotropy is strong (Figures 11(b)). For example, at coordinates $x = 12.0$ km and $z = 1.0$ km strong S wave residual exists, and at coordinates $x = 13.0$ km and $z = 1.5$ km strong P wave residual exists. VTI separators fail at locations where dip is large (Figures 11(c)). For example, at coordinates $x = 10.0$ km and $z = 1.2$ km strong S wave residual exits. However, even for this complicated model, separation using TTI separators is effective even at locations where medium parameter changes rapidly.

4. 3 3D VTI model

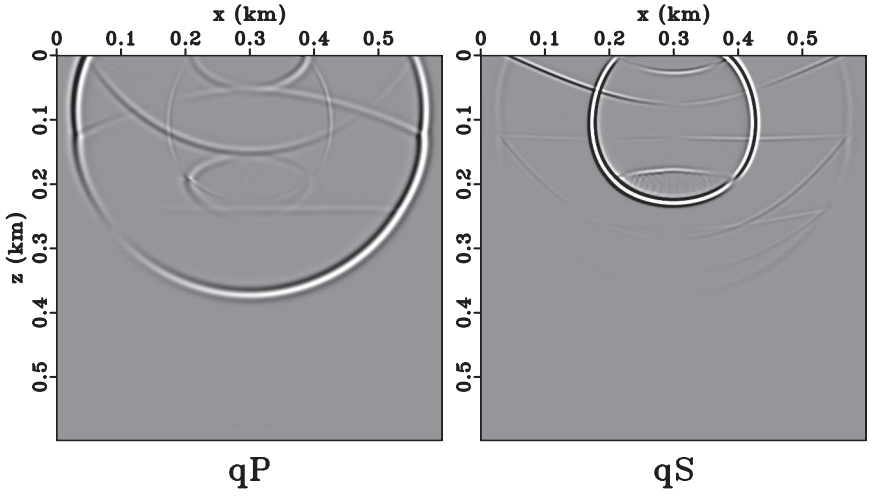
We show the 3D elastic wavefield separation using two examples.

Our first 3D example is a homogeneous isotropic model used to test the applicability of our convention used for the definition of polarization vectors in 3D media. The model has the parameters $V_{P0} = 3.5$ km/s, $V_{S0} = 1.75$ km/s, and $\rho = 2.0$ g/cm^3. Figure 12 shows a snapshot of the elastic wavefields in the z, x and y directions. A displacement source located at the center of the model oriented at vector direction $\{1, 1, 1\}$ is used to simulate the wavefields. Figure 13 shows well-separated P, SV, and SH modes using the algorithm described in the preceding sections. For 3D isotropic media, the S wave polarization is initially defined by the orientation of the source and SV and SH waves are defined relative to reflectors, and therefore, the polarization of SV and SH waves may change from location to location. Here, we make the convention that SV waves are polarized in vertical planes, and SH waves are polarized perpendicular to vertical planes. We use this model to test if the convention we define applies well to media with higher symmetry than TI models.

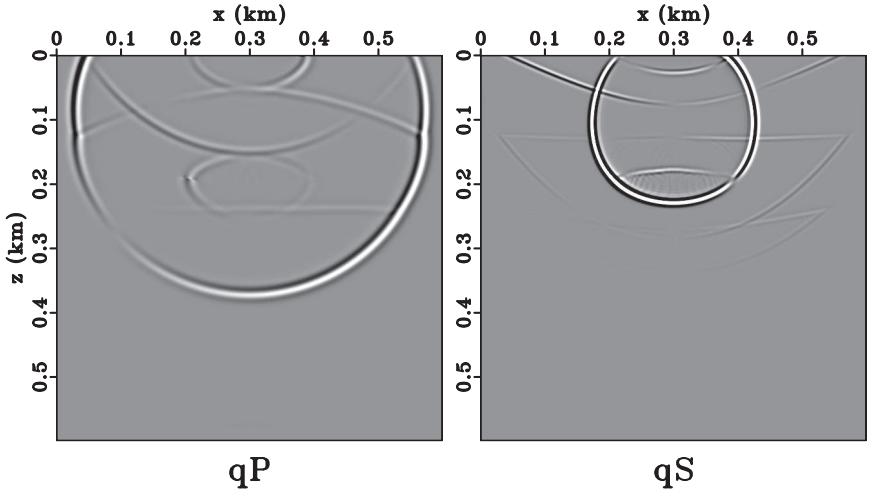
Our second example is a homogeneous VTI model used to illustrate the separation of 3D elastic wavefields. The model has the parameters $V_{P0} = 3.5$ km/s, $V_{S0} = 1.75$ km/s, $\rho = 2.0$ g/cm^3, $\epsilon = 0.4$, $\delta = 0.1$, and $\gamma = 0.0$. Figure 14 shows a snapshot of the elastic wavefields in the z, x and y directions. A displacement source located at the center of the model oriented at vector direction $\{1, 1, 1\}$ is used to simulate the wavefield. Figure 15 shows the separation into P, SV, and SH modes using the algorithm described above.



(a)



(b)



(c)

Figure 9. (a) A snapshot of the anisotropic wavefield simulated with a vertical point displacement source at $x = 0.3$ km and $z = 0.1$ km for the model shown in Figure 7, (b) anisotropic qP and qS modes separated using VTI pseudo-derivative operators and (c) anisotropic qP and qS modes separated using TTI pseudo-derivative operators. The separation of wavefields into qP and qS modes in (b) is not complete, which is visible such as at coordinates $x = 0.4$ km and $z = 0.9$ km. In contrast, the separation in (c) is better, because the correct anisotropic derivative operators are used.

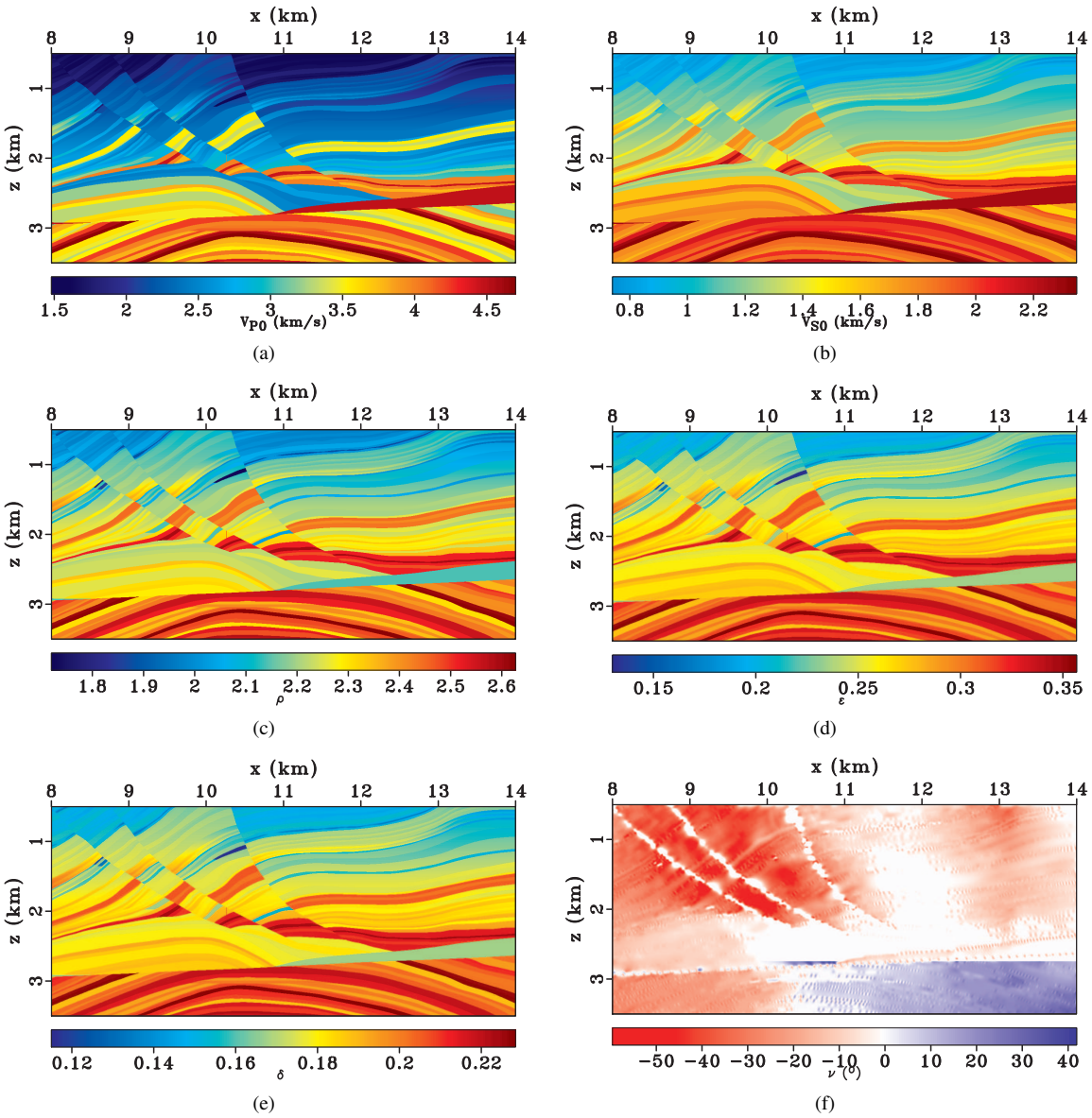


Figure 10. Anisotropic elastic Marmousi II model with (a) P wave velocity along the local symmetry axis, (b) S wave velocity along the local symmetry axis, (c) density, (d) ϵ, (e) δ, and (f) local tilt angle ν.

Because these two models are homogeneous, the separation is implemented in the k domain to reduce computation cost. For heterogeneous models, we can do non-stationary filtering in 3D to the wavefields to obtain separated wave modes.

5 DISCUSSION

5. 1 Computational issues

The separation of wave modes for heterogeneous TI media requires spatial non-stationary filtering with large operators, which is computationally expensive. The cost is directly proportional to the size of the model and the size of each operator. Furthermore, in a simple implementation, the storage for the separation operators of the entire model is proportional to the size of the model and the size of each operator. For a 3D VTI model of $300 \times 300 \times 300$ grid points, assuming that the operator has a size of $50 \times 50 \times 50$ samples, the storage for the operators is $(300)^3$ grid points $\times 50^3$ samples/independent operator $\times 4$ independent operators/grid point $\times 4$ Bytes/sample $= 54$ TB. This is not feasible for ordinary processing. However, since there are relative few medium parameters that control the properties of the operators, i.e., ϵ, δ, and V_P/V_S along the symmetry axis, we can construct a

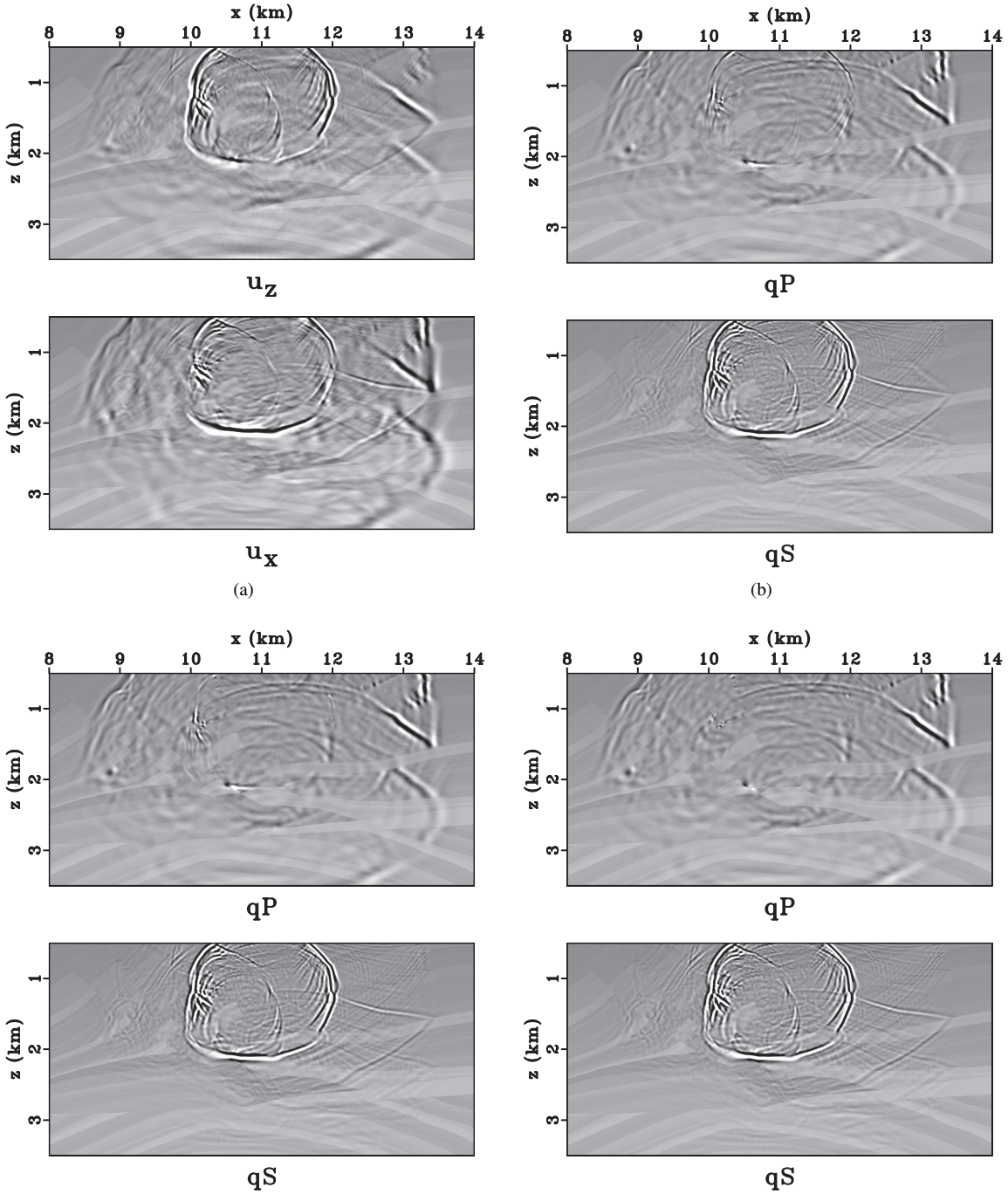


Figure 11. (a) A snapshot of the vertical and horizontal displacement wavefield simulated for model shown in Figure 10. Panels (b) to (c) are the P and SV wave separation using $\nabla \cdot$ and $\nabla \times$, VTI separators and TTI separators, respectively. The separation is incomplete in panel (b) and (c) where the model is strongly anisotropic and where the model tilt is large, respectively. Panel (d) shows the best separation among all.

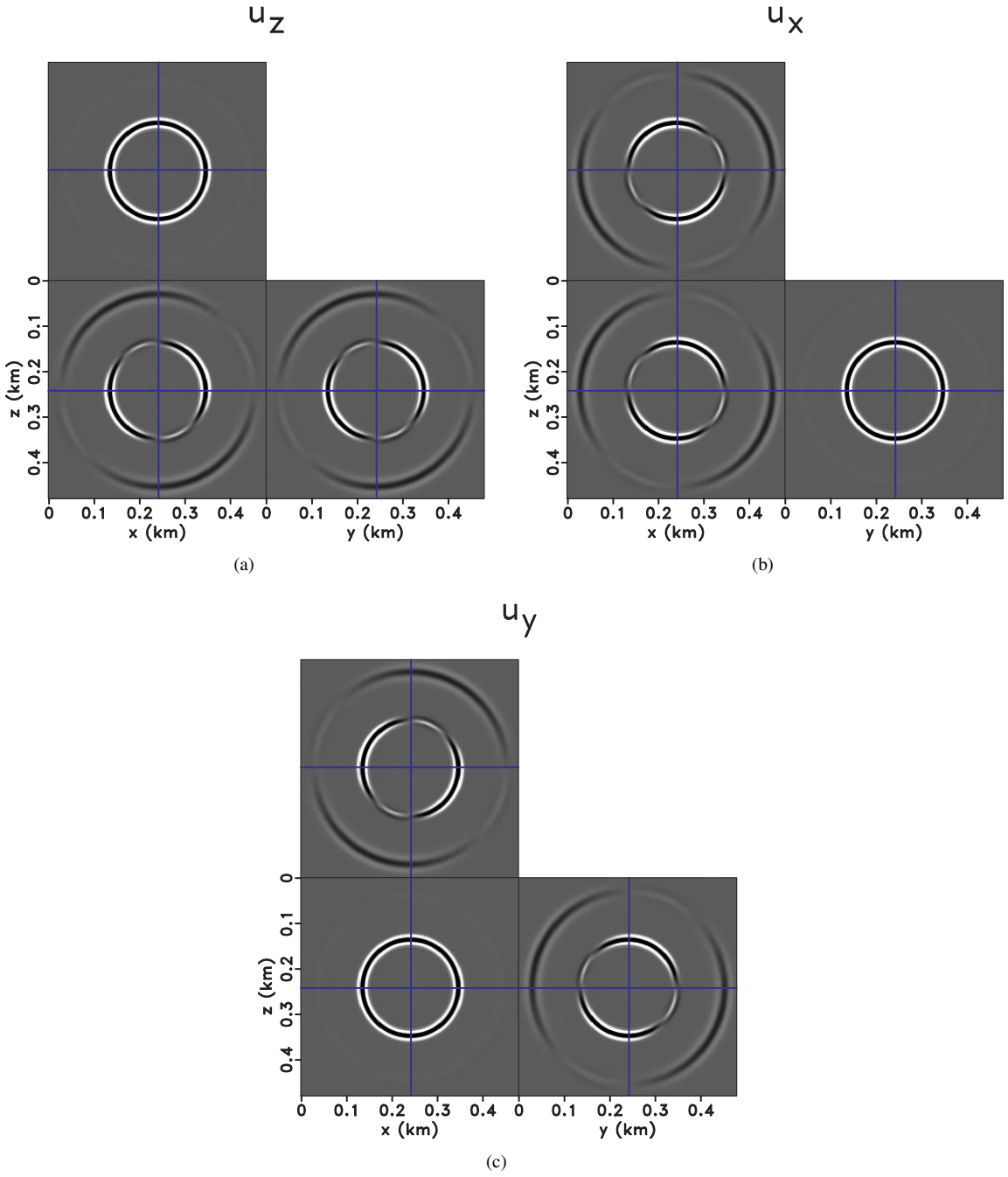


Figure 12. A snapshot of the elastic wavefield in the z, x and y directions for a 3D isotropic model. The model has parameters $V_{P0} = 3.5$ km/s, $V_{S0} = 1.75$ km/s, $\rho = 2.0$ g/cm^3. A displacement source located at the center of the model oriented at vector direction $\{1, 1, 1\}$ is used to simulate the wavefield.

table of operators as a function of these parameters, and select the appropriate operators at every location in space. For example, suppose we know that parameter $\epsilon \in [0, 0.3]$, $\delta \in [0, 0.1]$, and $V_P/V_S \in [1.5, 2.0]$, we can sample ϵ and δ at every 0.01 and V_P/V_S ratio along the symmetry axis at every 0.1. In this case, we only need a storage of $31 \times 11 \times 6$ combinations of medium parameters$\times 50^3$ sample/independent operator$\times 4$ independent operators/combination of medium parameters$\times$ 4 Bytes/sample $= 4$ GB, which is much more manageable.

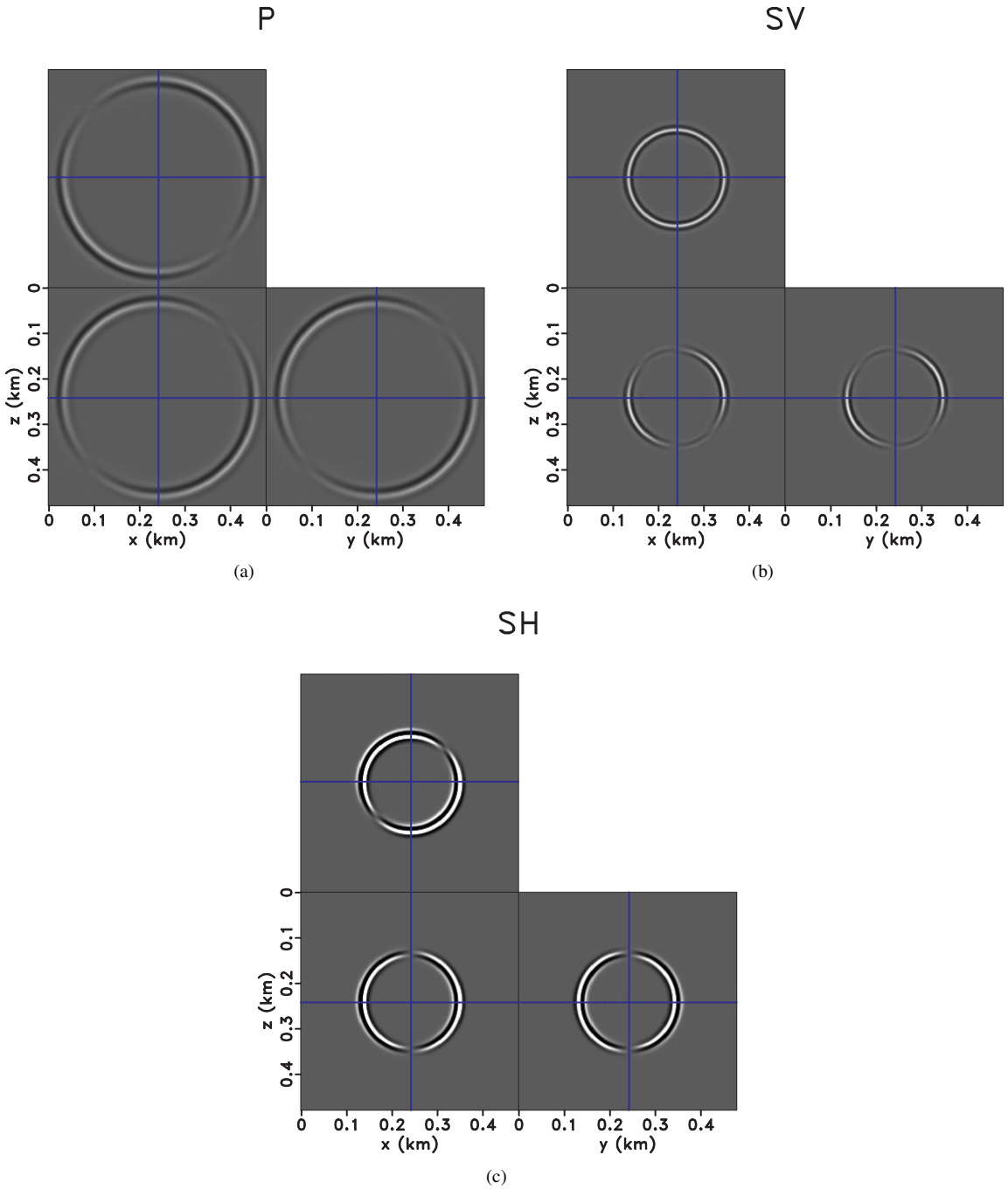


Figure 13. Separated P, SV and SH wave modes for the elastic wavefields shown in Figure 12. P, SV, and SH are well separated from each other.

5. 2 S mode amplitudes

Although the procedure used here to separate S waves into SV and SH modes is simple, the amplitudes of S modes are not correct due to the scaling factors in Equations 25 and 26. The amplitudes of S modes obtained in this way are zero in the symmetry axis direction and gradually increase to one in the symmetry plane. However, since the symmetry axis direction usually corresponds to normal incidence of the elastic waves, it is important to obtain more accurate S wave amplitudes in this direction. The main problem that impedes us from construct 3D global S-wave separators is that the SV and SH polarization vectors are singular in the symmetry axis direction, i.e., they are defined by plane-wave solution to the TI elastic wave equation. Various studies (Kieslev & Tsvankin,

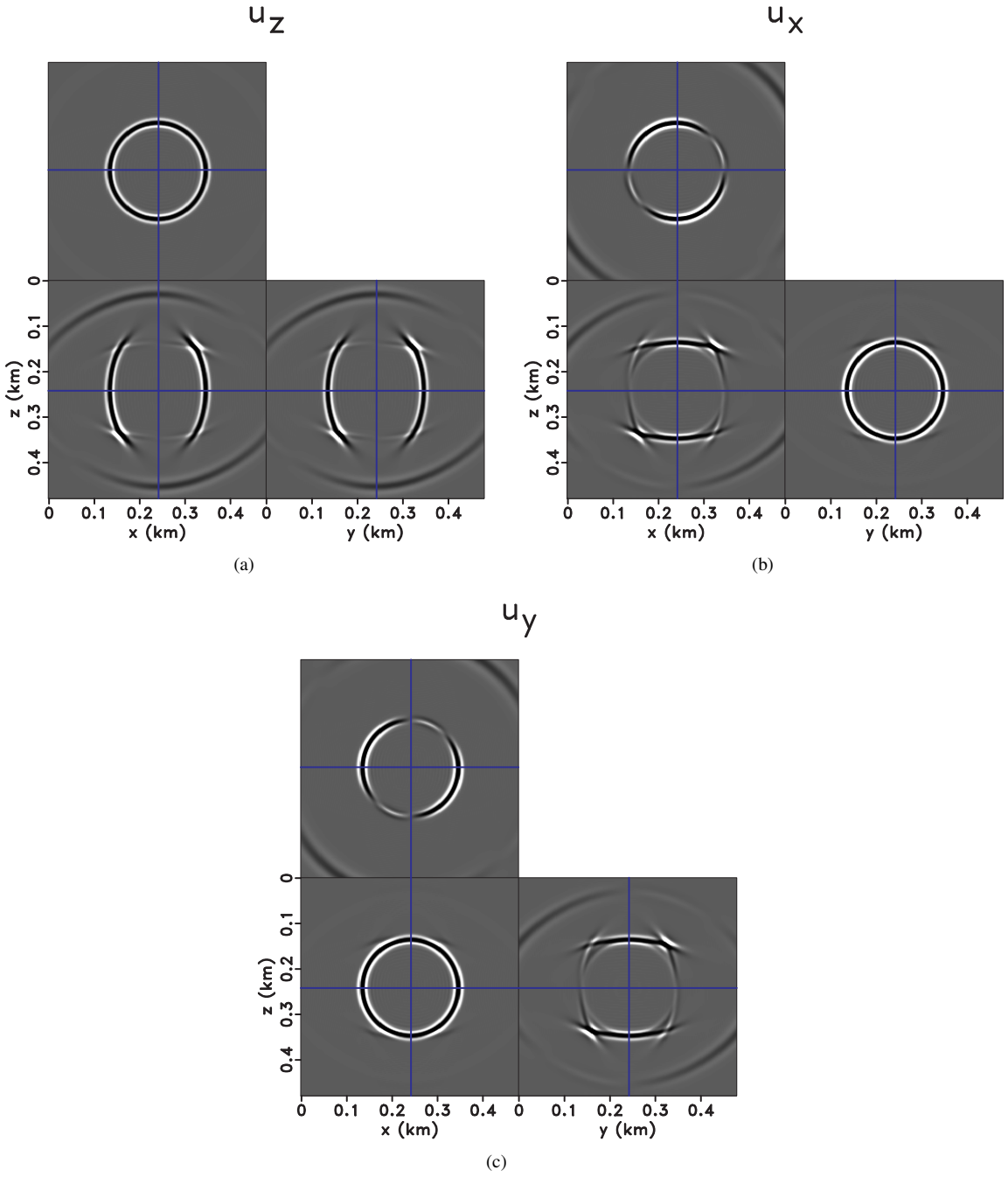


Figure 14. A snapshot of the elastic wavefield in the z, x and y directions for a 3D VTI model. The model has parameters $V_{P0} = 3.5$ km/s, $V_{S0} = 1.75$ km/s, $\rho = 2.0$ g/cm^3, $\epsilon = 0.4$, $\delta = 0.1$, and $\gamma = 0.0$. A displacement source located at the center of the model oriented at vector direction $\{1, 1, 1\}$ is used to simulate the wavefield.

1989; Tsvankin, 2005) show that S waves excited by point forces can have non-linear polarizations in several special directions. For example, in the direction of the force, S wave can deviate from linear polarization. This phenomenon exists even for isotropic media. Anisotropic velocity and amplitude variations can also cause S-wave to be polarized non-linearly. For instance, S-wave triplication, S-wave singularities, and S-wave velocity maximum can all result in S-wave polarization anomalies. In these special directions, SV and SH mode polarizations are probably incorrectly defined by our convention. One possibility to obtain more accurate S-wave amplitudes is to approximate the anomalous polarization with the major axes

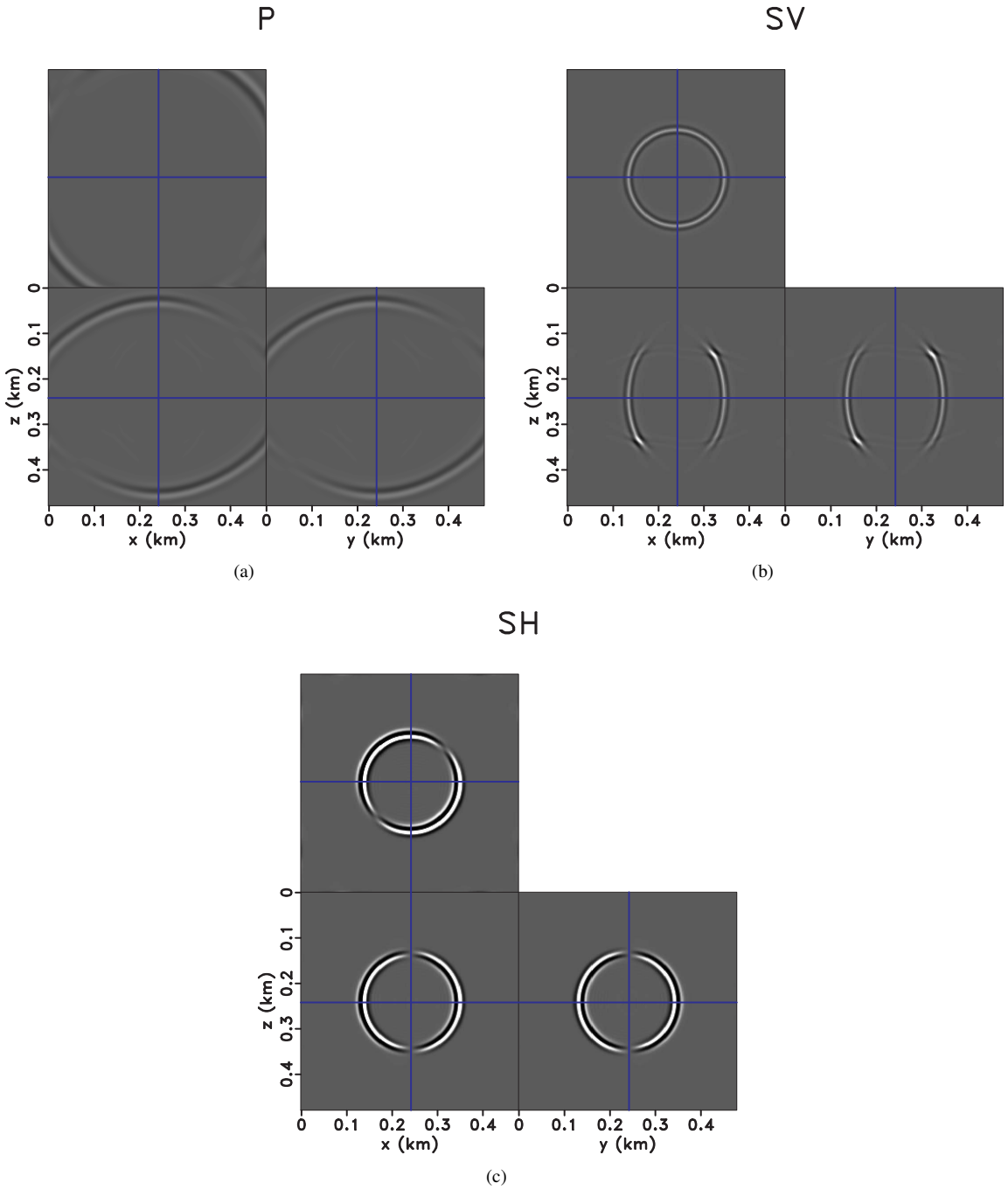


Figure 15. Separated P, SV and SH wave modes for the elastic wavefields shown in Figure 14. P, SV, and SH are well separated from each other.

of the quasi-ellipse of the S-wave polarization, which can be obtained incorporating the first-order term in the ray tracing method.

6 CONCLUSIONS

We present a method of obtaining spatially-varying derivative operators for TI models, which can be used to separate elastic wave modes in complex media. The main idea is to utilize polarization vectors constructed in the wavenumber domain using the local medium parameters and then transform these vectors back to the space domain. The main advantage of ap-

plying the derivative operators in the space domain constructed in this way is that they are suitable for heterogeneous media. In order for the operators to work for TTI models with non-zero tilt angles, we incorporate a parameter, local tilt angle ν, in addition to other parameters needed for the VTI operators.

We extend the wave mode separation to 3D TI models. The P, SV, and SH wavefield separators can all be constructed by solving the Christoffel equation for the P wave eigenvectors with local medium parameters. Constructing 3D separation operators saves us the processing step of decomposing the wavefields in azimuthally-dependent slices. The wave mode separators obtained using this method are spatially-variable filters and can be used to separate wavefields in TI media with arbitrary strength of anisotropy.

7 ACKNOWLEDGMENT

We acknowledge the support of the sponsors of the the Center for Wave Phenomena consortium project at the Colorado School of Mines.

REFERENCES

Aki, K., and Richards, P., 2002, Quantitative seismology (second edition): , University Science Books.

Alkhalifah, T., 1998, Acoustic approximations for processing in transversely isotropic media: Geophysics, **63**, no. 2, 623–631.

Alkhalifah, T., 2000, An acoustic wave equation for anisotropic media: Geophysics, **65**, no. 4, 1239–1250.

Behera, L., and Tsvankin, I., 2009, Migration velocity analysis and imaging for tilted TI media: Geophysical Prospecting, **57**, 13–26.

Bourgeois, A., Bourget, M., Lailly, P., Poulet, M., Ricarte, P., and Versteeg, R., 1991, The marmousi experience *in* Versteeg, R., and Grau, G., Eds., The Marmousi Experience, Proceedings of the 1990 EAEG workshop:, 5–16.

Chang, W. F., and McMechan, G. A., 1986, Reverse-time migration of offset vertical seismic profiling data using the excitation-time imaging condition: Geophysics, **51**, no. 1, 67–84.

Chang, W. F., and McMechan, G. A., 1994, 3-D elastic prestack, reverse-time depth migration: Geophysics, **59**, no. 4, 597–609.

Dellinger, J., and Etgen, J., 1990, Wave-field separation in two-dimensional anisotropic media (short note): Geophysics, **55**, no. 07, 914–919.

Dellinger, J., April 1991, Anisotropic seismic wave propagation: Ph.D. thesis, Stanford University.

Etgen, J. T., 1988, Prestacked migration of P and SV-waves: SEG Technical Program Expanded Abstracts, **7**, no. 1, 972–975.

Fletcher, R., Du, X., and Fowler, P. J., 2008, A new pseudo-acoustic wave equation for TI media: SEG Technical Program Expanded Abstracts, **27**, no. 1, 2082–2086.

Godfrey, R. J., 1991, Imaging Canadian foothills data: Imaging Canadian foothills data:, Soc. of Expl. Geophys., 61st Ann. Internat. Mtg, 207–209.

Gray, S. H., Etgen, J., Dellinger, J., and Whitmore, D., 2001, Seismic migration problems and solutions: Geophysics, **66**, no. 5, 1622–1640.

Hokstad, K., 2000, Multicomponent Kirchhoff migration: Geophysics, **65**, no. 3, 861–873.

Isaac, J. H., and Lawyer, L. C., 1999, Image mispositioning due to dipping TI media: A physical seismic modeling study: Geophysics, **64**, no. 4, 1230–1238.

Kieslev, A. P., and Tsvankin, I., 1989, A method of comparison of exact and asymptotic wave field computations: Geophysical Journal International, **96**, 253–258.

Shan, G., and Biondi, B., 2005, 3D wavefield extrapolation in laterally-varying tilted TI media: SEG Technical Program Expanded Abstracts, **24**, no. 1, 104–107.

Shan, G., 2006, Optimized implicit finite-difference migration for VTI media: SEG Technical Program Expanded Abstracts, **25**, no. 1, 2367–2371.

Thomsen, L., 1986, Weak elastic anisotropy: Geophysics, **51**, no. 10, 1954–1966.

Tsvankin, I., 2005, Seismic signatures and analysis of reflection data in anisotropic media: 2nd edition: , Elsevier Science Publ. Co., Inc.

Vestrum, R. W., Lawyer, L. C., and Schmid, R., 1999, Imaging structures below dipping TI media: Geophysics, **64**, no. 4, 1239–1246.

Yan, J., and Sava, P., 2008a, Elastic wavefield separation for VTI media: SEG Technical Program Expanded Abstracts, **27**, no. 1, 2191–2195.

——— 2008b, Isotropic angle-domain elastic reverse-time migration: Geophysics, **73**, no. 6, S229–S239.

Zhang, H. J., and Zhang, Y., 2008, Reverse time migration in 3D heterogeneous TTI media: SEG Technical Program Expanded Abstracts, **27**, no. 1, 2196–2200.

Zhe, J., and Greenhalgh, S. A., 1997, Prestack multicomponent migration: Geophysics, **62**, no. 02, 598–613.